

## ARTICLE OPEN

# A high-throughput technique for determining grain boundary character non-destructively in microstructures with through-thickness grains

Matteo Seita<sup>1</sup>, Marco Volpi<sup>2</sup>, Srikanth Patala<sup>3</sup>, Ian McCue<sup>4</sup>, Christopher A Schuh<sup>1</sup>, Maria Vittoria Diamanti<sup>2</sup>, Jonah Erlebacher<sup>4</sup> and Michael J Demkowicz<sup>5</sup>

Grain boundaries (GBs) govern many properties of polycrystalline materials. However, because of their structural variability, our knowledge of GB constitutive relations is still very limited. We present a novel method to characterise the complete crystallography of individual GBs non-destructively, with high-throughput, and using commercially available tools. This method combines electron diffraction, optical reflectance and numerical image analysis to determine all five crystallographic parameters of numerous GBs in samples with through-thickness grains. We demonstrate the technique by measuring the crystallographic character of about 1,000 individual GBs in aluminum in a single run. Our method enables cost- and time-effective assembly of crystallography–property databases for thousands of individual GBs. Such databases are essential for identifying GB constitutive relations and for predicting GB-related behaviours of polycrystalline solids.

npj Computational Materials (2016) 2, 16016; doi:10.1038/npjcompumats.2016.16; published online 24 June 2016

## INTRODUCTION

Polycrystalline materials are aggregates of differently oriented crystal grains joined along grain boundaries (GBs). Although they typically comprise a small fraction of the material's volume, GBs have tremendous impact on its properties, including strength and ductility,<sup>1–3</sup> thermal and electrical conductivity,<sup>4,5</sup> diffusion,<sup>6,7</sup> resistance to environment-assisted failure,<sup>8,9</sup> and radiation tolerance.<sup>10,11</sup> Although all grains may have identical crystal structure, GB structure depends at minimum on five crystallographic parameters:<sup>12,13</sup> three to describe the relative misorientation,  $\mathbf{R}$ , of the adjoining grains and two for the GB normal vector,  $\hat{n}$ .

A growing body of evidence shows that many GB properties,  $\phi$ , also depend on all five of these parameters.<sup>14–21</sup> Thus, we may write GB constitutive relations as  $\phi = F(\mathbf{R}, \hat{n})$ . Knowing these relations is key to predicting the behaviour of polycrystals and to designing materials with superior properties.<sup>22</sup> However, these relations are difficult to obtain experimentally because it is challenging to measure the property of interest,  $\phi$ , and the full character—i.e., both  $\mathbf{R}$  and  $\hat{n}$ —of numerous individual GBs. Measurement of GB properties, such as corrosion susceptibility, fracture strength or permeability, requires a physical test of the samples, which often irreversibly damages the GB or alters its character. Some techniques for determining GB character (GBC) involve the destruction of the sample, making it impossible to measure GB properties afterwards.

We have developed a new high-throughput method to measure GBC without altering the samples and thus allowing further testing to assess properties of individual GBs. Our method relies on the preparation of microstructures with through-thickness

grains and integrates measurements of  $\mathbf{R}$  through electron backscatter diffraction (EBSD)<sup>23</sup> with determinations of  $\hat{n}$  using optical reflectance microscopy (ORM).<sup>24</sup> a hybrid technique we term EDOR (electron diffraction optical reflectance). We demonstrate and validate EDOR on GBs in polycrystalline aluminum (Al). EDOR may be employed to collect the large experimental data sets needed to establish GB constitutive relations,  $\phi = F(\mathbf{R}, \hat{n})$ .

Although the misorientation of GBs on free surfaces is easy to measure non-destructively using EBSD,<sup>23</sup> finding GB plane normal vectors is usually harder.<sup>25</sup> One approach to obtain them couples EBSD with focused ion-beam serial sectioning.<sup>26</sup> Although this is a versatile technique that may be employed on a wide range of microstructures and sample geometries, it requires the physical destruction of the GBs to measure their character, which prevents any further test aimed at measuring their physical properties. GBC may be found using transmission electron microscopy<sup>20</sup> or three-dimensional X-ray diffraction (3DXRD)<sup>27–29</sup> while leaving GBs available, in principle, for subsequent property measurements. However, transmission electron microscopy has limited throughput—it can only study a few GBs at a time—whereas 3DXRD is cost- and time-intensive—it requires advanced X-ray sources and significant computational effort to reconstruct GBC.<sup>30</sup> The advantage of EDOR over these techniques is its ability to assess GBC non-destructively, with high-throughput, and using commercially available equipment and software.

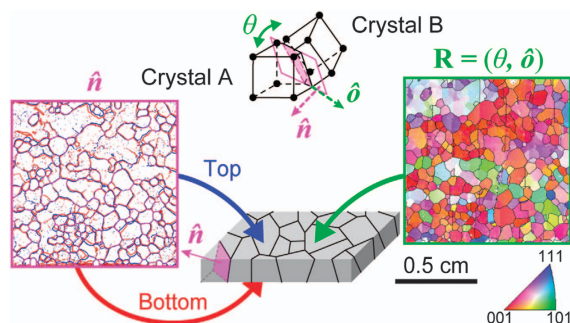
## RESULTS

Figure 1 illustrates the elements of EDOR. The method is intended for samples with through-thickness grains. Many commonly

<sup>1</sup>Department of Materials Science and Engineering, Massachusetts Institute of Technology, Cambridge, MA, USA; <sup>2</sup>Department of Chemistry, Materials and Chemical Engineering 'G Natta', Politecnico di Milano, Milan, Italy; <sup>3</sup>Department of Materials Science and Engineering, North Carolina State University, Raleigh, NC, USA; <sup>4</sup>Department of Materials Science and Engineering, Johns Hopkins University, Baltimore, MD, USA and <sup>5</sup>Materials Science and Engineering, Texas A&M University, College Station, TX, USA. Correspondence: M Seita (matteos@mit.edu)

Received 9 December 2015; revised 18 May 2016; accepted 20 May 2016

encountered types of samples have such microstructures, including films that have been epitaxially grown and then lifted off of their substrates<sup>31</sup> or polycrystals that have been mechanically thinned into foils with thickness smaller than the average grain size.<sup>8</sup> Not all such samples are representative of bulk microstructures. However, our work is not aimed at investigating bulk microstructure, but rather at relating the crystallographic character of numerous individual GBs to their physical properties. Samples with through-thickness grains provide rich data sets to study these relationships, provided that the GBs within them sample a broad range of GBCs. Here we illustrate EDOR using engineered Al foils with through-thickness grains created by repeated rolling and annealing (see the Methods section). The foils are  $\sim 600\text{-}\mu\text{m}$  thick and contain grains with average diameter of



**Figure 1.** EDOR process to assess GB crystallography (top schematics) using through-thickness-grained microstructures. Left: optical reflectance micrographs taken from the top and bottom of the sample are used to evaluate the GB plane normal vector. Right: EBSD characterisation on the top side of the sample is used to measure GB misorientation.

$\sim 700\text{ }\mu\text{m}$ . EDOR consists of (1) the non-destructive characterisation of the GB plane normal vectors  $\hat{n}$  using ORM, (2) assessment of the GB misorientation using EBSD and (3) integration of these two data sets into a list of complete GBCs for all GBs in the sample.

In the first step, the GB plane normal vector  $\hat{n}$  in the laboratory frame is measured by analysing both sides of the sample through ORM—a process illustrated in Figure 2. To reveal the crystallographic facets of the constituent grains, both sides of the sample are mechanically polished and then chemically etched (see the Methods section). A sequence of micrographs is acquired from both sides of the engineered sample under variable incident light direction using a stereographic optical microscope, as shown in Figure 2a. The reflectance of a grain along a specific direction depends on the orientation of the crystallographic facets on its surface with respect to the incoming light.<sup>24</sup> Thus, different grains appear with different intensity through the optical microscope as a function of both their crystallographic orientation and the direction of the incident light (Figure 2a). Each optical micrograph is then digitally segmented using a MATLAB processing routine (described in detail in Supplementary Information) that finds the GB traces on the sample surfaces using a contrast-based edge detection algorithm,<sup>32</sup> as illustrated in Figure 2b. The algorithm identifies GB traces by detecting discontinuities in intensity that are larger than a pre-specified threshold. This image processing routine detects all GBs in the microstructure, where a GB is defined by a crystallographic misorientation of  $\theta \geq 5^\circ$ , as in other techniques.<sup>23</sup>

Not all GBs appear in each optical micrograph. Acquiring multiple optical micrographs under different illumination conditions ensures that all GBs are detected in at least one of them. The digitalised micrographs are then summed into two cumulative ‘TOP’ and ‘BOTTOM’ micrographs that contain all detected GB traces from both sample sides, shown in Figure 2c. To remove noise arising from surface scratches or irregularities,

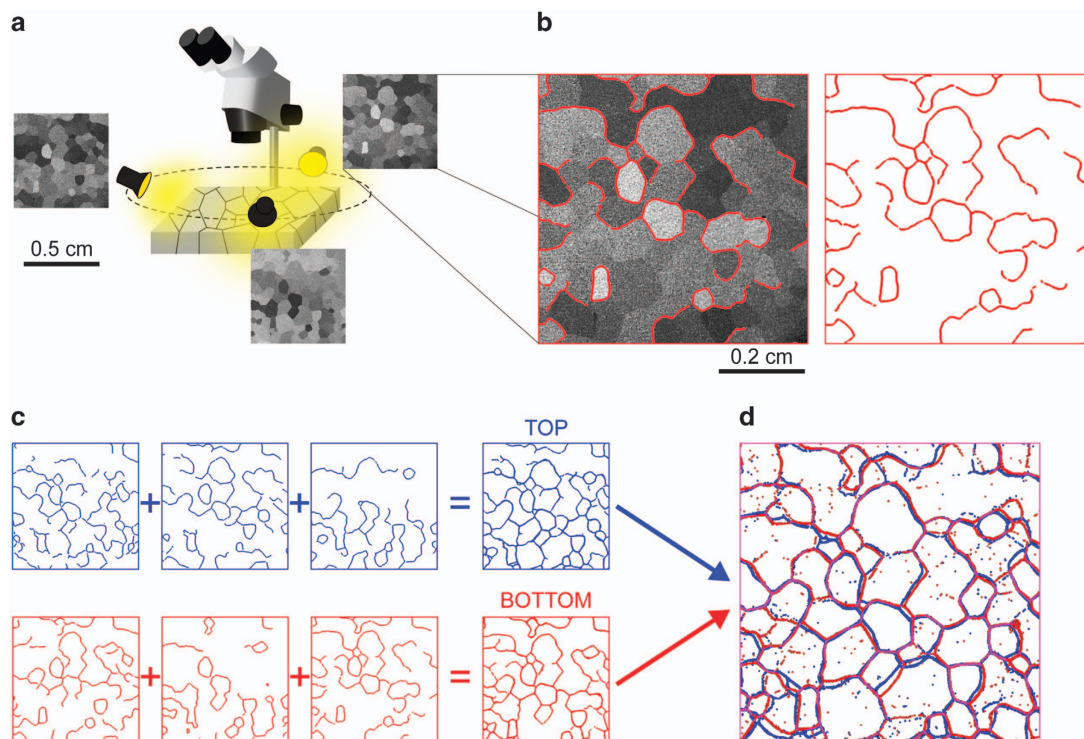


**Figure 2.** Evaluating GB plane normal vectors. (a) Acquisition of a sequence of optical micrographs under different illumination conditions. (b) Post-processing of each optical micrograph to detect GB traces using a contrast-based edge detection algorithm. (c) Reconstruction of the GB trace network from the top (blue) and bottom (red) of the sample by summing the sequence of processed optical micrographs. (d) Registration of the cumulative ‘TOP’ and ‘BOTTOM’ images to display the projected GB network (overlapping signal between TOP and BOTTOM displayed in purple). For interpretation of colours, the reader is referred to the web version of this article.

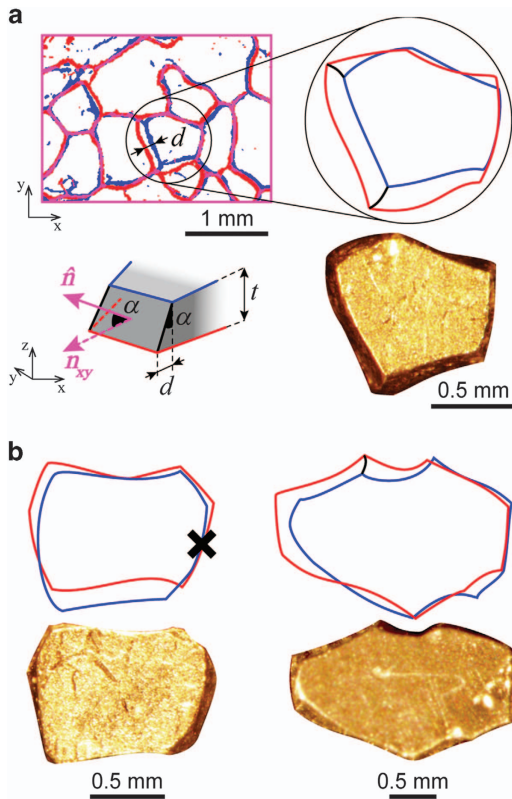


**Figure 3.** Calculation and validation of GB plane tilt angle  $\alpha$ . **(a)** Evaluation of the distance  $d$  between top- and bottom-GB traces. The 3D schematic shows the orientation of the GB plane in the laboratory reference frame. **(b)** Comparison of grain shapes obtained through EDOR with direct images of the same grains after disaggregation of the Al microstructure via Ga permeation. The GB crossed in black is the only instance where the EDOR prediction does not match the actual plane tilt.

all features that have low cumulative signal are filtered out. This way, all GB traces from both top and bottom sides of the sample are found, with the exception of those that appear with low frequency in the cumulative images (Supplementary Information). TOP and BOTTOM are then registered in MATLAB using pre-fabricated fiducial markers: through-thickness notches engraved by electric discharge machining around the perimeter of the sample (Supplementary Information). Registration may be performed manually by selecting control points at the notch vertices or automatically using a built-in MATLAB function that uses an intensity-based registration algorithm. The result is a single micrograph, shown in Figure 2d, that contains GB traces from both top and bottom sides of the engineered sample.

To evaluate the normal vector  $\hat{n}$ , we follow the procedure illustrated in Figure 3a. The tilt angle  $\alpha$  of the GB plane with respect to the top surface is computed from the sample thickness  $t$  at the GB location and the average distance  $d$  between the GB traces on the top and bottom sides:

$$\alpha = \arctan\left(\frac{d}{t}\right). \quad (1)$$

$t$  is estimated by interpolating the thickness values measured around the perimeter of the samples using a caliper, whereas  $d$  is computed automatically from the registered micrograph shown in Figure 2d (Supplementary Information). The GB plane normal vector  $\hat{n}$  (in the lab frame) may then be written as:

$$\hat{n} = \left[ \frac{n_x}{\sqrt{n_x^2 + n_y^2}} \cos(\alpha) \hat{x} \quad \frac{n_y}{\sqrt{n_x^2 + n_y^2}} \cos(\alpha) \hat{y} \quad |\sin(\alpha)| \hat{z} \right] \quad (2)$$

$n_x$  and  $n_y$  are measured from the linear fit to the top GB trace. We adopt the convention that the normal vector,  $\hat{n}$ , points from the bottom side to the top.

To test the accuracy of this calculation, we permeate our Al sample with liquid gallium (Ga; Supplementary Information). Permeation of Ga into Al is intergranular and leads to the disaggregation of the microstructure into constituent grains without altering the grain shapes.<sup>33</sup> We confirm the GB plane tilts calculated using EDOR by imaging individual grains using optical microscopy. Three illustrative grains are shown in Figure 3b. The measurement error,  $\Delta\alpha$ , in the computed GB plane tilt may arise from neglecting possible out-of-plane curvature of the boundary plane, from uncertainties in the evaluation of the GB trace distance,  $\Delta d$ , and from local variations in sample thickness,  $\Delta t$ , that result from non-uniform grinding during sample preparation. We inspect selected grain facets by scanning electron microscopy and find that the out-of-plane curvature is negligible over the length of the GB (see Supplementary Figure S14 in the Supplementary Information). Following equation (1), we have

computed an error of  $\Delta\alpha = \frac{\sqrt{t^2 \Delta d^2 + d^2 \Delta t^2}}{(d^2 + t^2)} \approx 3^\circ$  using conventional uncertainty propagation techniques (Supplementary Information).

In the second step of EDOR, we find GB misorientations. The top side of the sample is prepared for EBSD characterisation (see the Methods section). The EBSD data set is imported into MATLAB through MTEX,<sup>34</sup> a toolbox used to compute misorientation angles  $\theta$  and axes  $\hat{o}$  of each GB from the crystallographic orientation of the adjoining grains. In principle, EBSD or other electron-based microscopy techniques, such as orientation contrast imaging,<sup>35</sup> may also be conducted on both sides of the sample and then used to reconstruct the GB network—similar to how ORM operates in EDOR—or else performed on one side of the sample only and then combined with Monte Carlo simulations to infer the likeliest GB plane normal vector.<sup>36</sup> These approaches are advantageous in that they all use scanning electron microscopy and do not require registration of different data sets. However, they are mostly suitable for small-size samples and become impractical for large samples due to EBSD's and orientation contrast imaging's limited field of view, slow scanning speed and large image distortion.<sup>37</sup> For these reasons, EDOR relies on optical—rather than electron-based—techniques to assess GB plane normal vectors.

Finally, in the third step of EDOR, the EBSD data ( $\theta$  and  $\hat{o}$  as well as the orientations of the two adjacent grains,  $O_A$  and  $O_B$ ) are automatically assigned to the corresponding GB plane normal vector  $\hat{n}$ , such that for each GB both the misorientation and plane normal vector are specified. This procedure is detailed in the Supplementary Information. The grain orientations obtained with EBSD are used to rotate the GB plane normal vector  $\hat{n}$  from the lab frame into the frames of the individual grains:  $\hat{n}_A$  and  $\hat{n}_B$ :

$$\begin{aligned} \hat{n}_A &= O_A^{-1} \cdot \hat{n} \\ \hat{n}_B &= O_B^{-1} \cdot \hat{n} \end{aligned} \quad (3)$$

$\hat{n}_A$  and  $\hat{n}_B$  are representations of the same GB plane, expressed with respect to reference frames fixed to the two adjoining crystal grains. In this paper, we use both  $\hat{n}_A$  and  $\hat{n}_B$  for representing each measured GB plane. We note that a unique representation of the GBC—considering both misorientation and boundary plane—can be found after considering all symmetry operations that stem from the underlying crystals.<sup>38</sup> The implications of using such a representation on the formulation of GB constitutive relations will be discussed in a future publication.

## DISCUSSION

Using EDOR, we found the complete GBC of 976 GBs from three Al samples with cumulative area of  $\sim 1.4 \text{ cm}^2$ . Figure 4 presents the disorientations—using the axis-angle parameterisation—(Figure 4a) and boundary plane orientations (Figure 4b) of these GBs,



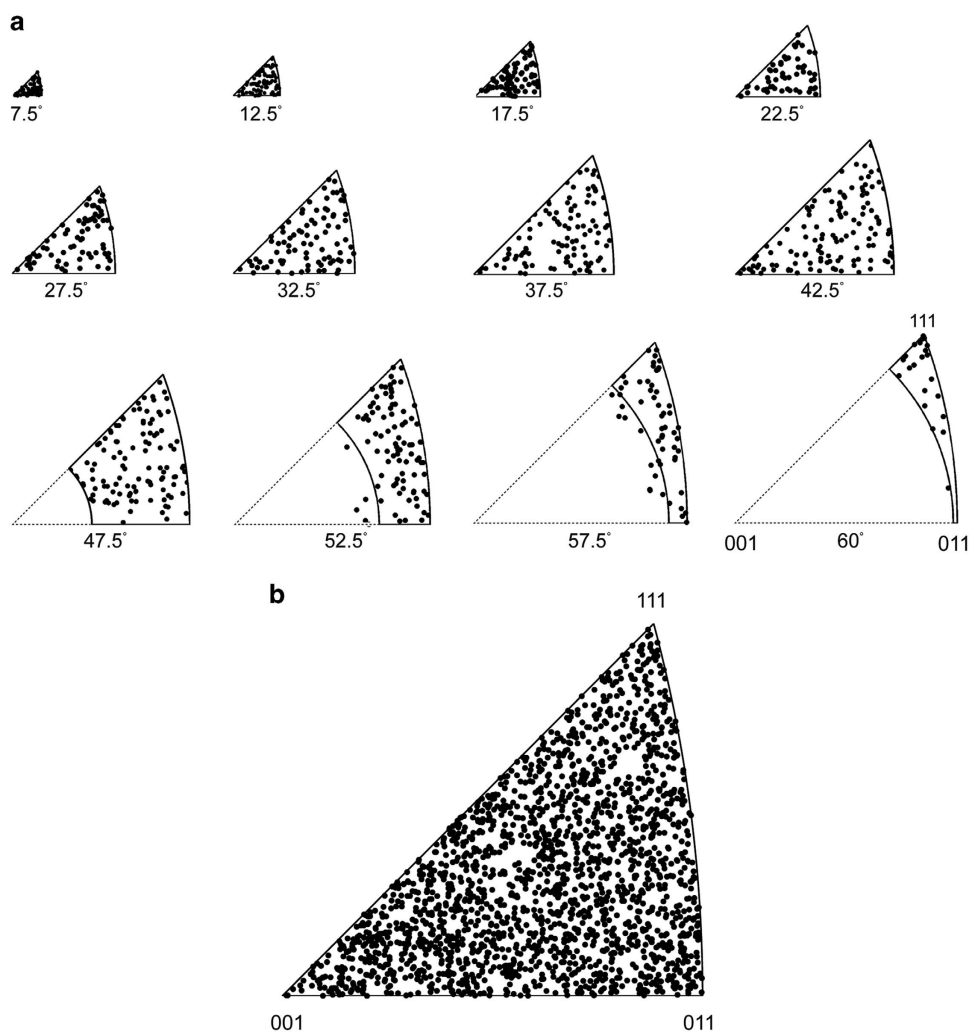


**Figure 4.** Visualisation of the GBC distribution as measured by EDOR in polycrystalline Al. **(a)** GB misorientation distribution. The plot shows progressive slices of constant  $\theta$  through the asymmetric fundamental zone for misorientations in cubic crystals. Each section comprises GBs within the specified range of  $\theta \pm 2.5^\circ$  (indicated in degrees below each slice).<sup>43</sup> **(b)** Distribution of the GB plane normal vectors plotted in the standard stereographic triangle for cubic symmetry.

showing an approximately uniform and diverse sampling of GBC. The misorientation distribution function of one representative Al sample is also reported in the Supplementary Information. All three Al samples remained undamaged by these measurements and were therefore available for subsequent measurements of GB properties. These results demonstrate that EDOR is a reliable, high-throughput and non-destructive technique to assess the GBC of numerous individual GBs in polycrystalline materials. It therefore provides a critical capability for finding GB crystallography–property relationships,  $\phi = F(\mathbf{R}, \hat{n})$ . Owing to its hybrid nature—which combines ORM and EBSD—EDOR has higher versatility than other optical techniques and may therefore be applied to a wider range of materials.<sup>39</sup> As it relies on commercially available equipment and software, EDOR may be widely adopted by many groups to study GB crystallography–property relations. The MATLAB scripts for EDOR as well as the raw data presented in this paper are provided in the Supplementary Information. As a proof of concept, we employed EDOR on Al samples created by repeated rolling and annealing. However, EDOR may also be employed on other types of samples, with grain size resolvable by ORM and sample thickness smaller than the average grain size. Modified versions of EDOR may be employed to characterise nanostructured materials or thin films by means of transmission electron microscopy,<sup>40,41</sup> or as an *in situ* characterisation tool in

layer-by-layer additive manufacturing.<sup>42</sup> Further improvements to EDOR will aim at retrieving GB misorientations using ORM and at meshing the surface of curved GBs to extract variable GB plane normals.<sup>27</sup> These upgrades will significantly improve the efficiency of EDOR at sampling the GB crystallography space, by removing the need for EBSD—the most time-intensive step in EDOR—and maximising the number of detected GBs per sample.

## MATERIALS AND METHODS

Al samples with through-thickness grains were produced from a 500-g high-purity Al (99.999%) master ingot. A  $\sim 20$ -mm-thick foil was cut from the master ingot and underwent a series of rolling and annealing cycles until the foil was  $\sim 600$ - $\mu\text{m}$  thick. Each cycle consisted of a 50% thickness reduction, chemical etching in 1 mol/l NaOH solution at 80 °C for 15 min, and annealing at 620 °C for 20 min. The amount of thickness reduction was tailored to ensure complete recrystallisation upon annealing, while limiting texture formation and minimising work hardening. The chemical etching was used to remove the native oxide film that may form at each cycle and contaminate the rollers. The annealing temperature was chosen near the melting temperature of Al to maximise the kinetics of grain growth. Both sides of the Al samples with through-thickness grains were then mechanically polished using a sequence of SiC paper from 2,400 to 4,000 grit size. Subsequently, the samples were immersed in a bath of 1 N NaOH for 30 min in stirring condition to reveal the crystallographic facets of the

constituent grains. After having characterised the microstructure by optical reflectance, one side of the sample (referred to as the top side) was further polished using a colloidal silica suspension (0.04  $\mu\text{m}$ ) to a mirror-like quality and then characterised by EBSD.

## ACKNOWLEDGEMENTS

We acknowledge O.K. Johnson for providing help with the MATLAB code and for stimulating discussions. This work was supported by the US Department of Energy, Office of Basic Energy Sciences under award no DE-SC0008926. M.V. was supported by the MITI Seed Fund 'Progetto Roberto Rocca.' I.M. and J.E. were supported by the National Science Foundation under grant DMR-1003901. Access to shared experimental facilities was provided by the MIT Center for Materials Science Engineering.

## CONTRIBUTIONS

The project was planned and supervised by M.S., M.J.D., M.V.D. and C.A.S. EDOR was conceived by M.S. Data collection and analysis were performed by M.S. and M.V. The MATLAB code was written by M.S. and S.P. Samples were designed by J.E. and prepared by I.M. The manuscript was prepared by M.S., S.P. and M.J.D.

## COMPETING INTERESTS

The authors declare no conflict of interest.

## REFERENCES

- Lu, K., Lu, L. & Suresh, S. Strengthening materials by engineering coherent internal boundaries at the nanoscale. *Science* **324**, 349–352 (2009).
- Lu, L., Chen, X., Huang, X. & Lu, K. Revealing the maximum strength in nanotwinned copper. *Science* **323**, 607–610 (2009).
- Wei, Y. J. *et al.* Evading the strength–ductility trade-off dilemma in steel through gradient hierarchical nanotwins. *Nat. Commun.* **5**, 3580 (2014).
- Minnich, A. J., Dresselhaus, M. S., Ren, Z. F. & Chen, G. Bulk nanostructured thermoelectric materials: current research and future prospects. *Energy Environ. Sci.* **2**, 466–479 (2009).
- Cook B. A., Kramer M. J., Wei X., Harringa J. L. & Levin E. M. Nature of the cubic to rhombohedral structural transformation in (AgSbTe<sub>2</sub>)<sub>15</sub>(GeTe)<sub>85</sub> thermoelectric material. *J. Appl. Phys.* **101**, 053715 (2007).
- Suzuki, A. & Mishin, Y. Diffusion mechanisms in grain boundaries in conventional and nanostructured materials. *Minerals, Metals & Materials Soc.* 43–60 (2004).
- Chen, Y. & Schuh, C. A. Diffusion on grain boundary networks: percolation theory and effective medium approximations. *Acta Mater.* **54**, 4709–4720 (2006).
- Seita, M., Hanson, J. P., Gradecak, S. & Demkowicz, M. J. The dual role of coherent twin boundaries in hydrogen embrittlement. *Nat. Commun.* **6**, 6164 (2015).
- Lehockey, E. M. *et al.* On improving the corrosion and growth resistance of positive Pb-acid battery grids by grain boundary engineering. *J. Power Sources* **78**, 79–83 (1999).
- Shen T. D. *et al.* Enhanced radiation tolerance in nanocrystalline MgGa<sub>2</sub>O<sub>4</sub>. *Appl. Phys. Lett.* **90**, 263115 (2007).
- Uberuaga, B. P., Vernon, L. J., Martinez, E. & Voter, A. F. The relationship between grain boundary structure, defect mobility, and grain boundary sink efficiency. *Sci. Rep.* **5**, 9095 (2015).
- Sutton, A. P. & Balluffi, R. W. *Interfaces in crystalline materials*. (Oxford University Press, New York, NY, USA, 2007).
- Rohrer, G. S. The distribution of grain boundary planes in polycrystals. *JOM* **59**, 38–42 (2007).
- Kaur, I., Mishin, Y. & Gust, W. *Fundamentals of Grain and Interphase Boundary Diffusion*. (John Wiley & Sons, Chichester, UK, 1995).
- Mishin, Y., Asta, M. & Li, J. Atomistic modeling of interfaces and their impact on microstructure and properties. *Acta Mater.* **58**, 1117–1151 (2010).
- Rohrer, G. S. *et al.* Comparing calculated and measured grain boundary energies in nickel. *Acta Mater.* **58**, 5063–5069 (2010).
- Olmsted, D. L., Holm, E. A. & Foiles, S. M. Survey of computed grain boundary properties in face-centered cubic metals-II: Grain boundary mobility. *Acta Mater.* **57**, 3704–3713 (2009).
- Olmsted, D. L., Foiles, S. M. & Holm, E. A. Survey of computed grain boundary properties in face-centered cubic metals: I. Grain boundary energy. *Acta Mater.* **57**, 3694–3703 (2009).
- Holm, E. A. & Foiles, S. M. How Grain Growth Stops: A Mechanism for Grain-Growth Stagnation in Pure Materials. *Science* **328**, 1138–1141 (2010).
- Hugo, R. C. & Hoagland, R. G. The kinetics of gallium penetration into aluminum grain boundaries—In situ TEM observations and atomistic models. *Acta Mater.* **48**, 1949–1957 (2000).
- Han, W. Z., Demkowicz, M. J., Fu, E. G., Wang, Y. Q. & Misra, A. Effect of grain boundary character on sink efficiency. *Acta Mater.* **60**, 6341–6351 (2012).
- Vattre, A. J., Abdolrahim, N., Kolluri, K. & Demkowicz, M. J. Computational design of patterned interfaces using reduced order models. *Sci. Rep.* **4**, 6231 (2014).
- Adams, B. L., Wright, S. I. & Kunze, K. Orientation imaging—the emergence of a new microscopy. *Metall. Trans. A* **24**, 819–831 (1993).
- Weightman, P., Martin, D. S., Cole, R. J. & Farrell, T. Reflection anisotropy spectroscopy. *Rep. Prog. Phys.* **68**, 1251–1341 (2005).
- Rohrer, G. S. *et al.* The distribution of internal interfaces in polycrystals. *Z. Metallkd.* **95**, 197–214 (2004).
- Khorashadzadeh, A. *et al.* Five-Parameter Grain Boundary Analysis by 3D EBSD of an Ultra Fine Grained CuZr Alloy Processed by Equal Channel Angular Pressing. *Adv. Eng. Mater.* **13**, 237–244 (2011).
- Lieberman, E. J., Rollett, A. D., Lebensohn, R. A. & Kober, E. M. Calculation of grain boundary normals directly from 3D microstructure images. *Model. Simul. Mater. Sci.* **23**, 035005 (2015).
- King, A., Johnson, G., Engelberg, D., Ludwig, W. & Marrow, J. Observations of intergranular stress corrosion cracking in a grain-mapped polycrystal. *Science* **321**, 382–385 (2008).
- Poulsen, H. F. *et al.* Three-dimensional maps of grain boundaries and the stress state of individual grains in polycrystals and powders. *J. Appl. Crystallogr.* **34**, 751–756 (2001).
- Suter R. M., Hennessy D., Xiao C. & Lienert U. Forward modeling method for microstructure reconstruction using x-ray diffraction microscopy: Single-crystal verification. *Rev. Sci. Instrum.* **77**, 123905 (2006).
- Rupert, T. J., Gianola, D. S., Gan, Y. & Hemker, K. J. Experimental observations of stress-driven grain boundary migration. *Science* **326**, 1686–1690 (2009).
- Canny, J. A computational approach to edge detection. *IEEE Trans. Pattern Anal. Mach. Intell.* **PAMI-8**, 679–698 (1986).
- Joseph, B., Picat, M. & Barbier, F. Liquid metal embrittlement: a state-of-the-art appraisal. *Eur. Phys. J. Appl. Phys.* **5**, 19–31 (1999).
- Bachmann, F., Hielscher, R. & Schaeben, H. Texture analysis with MTEX—free and open source software toolbox. *Solid State Phenom.* **160**, 63–68 (2010).
- Prior, D. J., Trimby, P. W., Weber, U. D. & Dingley, D. J. Orientation contrast imaging of microstructures in rocks using foreshatter detectors in the scanning electron microscope. *Mineral. Mag.* **60**, 859–869 (1996).
- Sorensen, C., Basinger, J. A., Nowell, M. M. & Fullwood, D. T. Five-parameter grain boundary inclination recovery with EBSD and interaction volume models. *Metall. Mater. Trans. A* **45**, 4165–4172 (2014).
- Pilchak, A. L., Shiveley, A. R., Shade, P. A., Tiley, J. S. & Ballard, D. L. Using cross-correlation for automated stitching of two-dimensional multi-tile electron backscatter diffraction data. *J. Microsc.* **248**, 172–186 (2012).
- Patala, S. & Schuh, C. A. Symmetries in the representation of grain boundary-plane distributions. *Philos. Mag.* **93**, 524–573 (2013).
- Heilbronner, R. P. & Pauli, C. Integrated spatial and orientation analysis of quartz c-axes by computer-aided microscopy. *J. Struct. Geol.* **15**, 369–382 (1993).
- Ghamarian, I., Liu, Y., Samimi, P. & Collins, P. C. Development and application of a novel precession electron diffraction technique to quantify and map deformation structures in highly deformed materials—as applied to ultrafine-grained titanium. *Acta Mater.* **79**, 203–215 (2014).
- Rauch, E. F. & Veron, M. Automated crystal orientation and phase mapping in TEM. *Mater. Charact.* **98**, 1–9 (2014).
- Dinwiddie, R. B., Dehoff, R. R., Lloyd, P. D., Lowe, L. E. & Ulrich, J. B. Thermographic in-situ process monitoring of the electron beam melting technology used in additive manufacturing. *Proc. SPIE* **8705K**, 1–8 (2013).
- Patala, S., Mason, J. K. & Schuh, C. A. Improved representations of misorientation information for grain boundary science and engineering. *Prog. Mater. Sci.* **57**, 1383–1425 (2012).



This work is licensed under a Creative Commons Attribution 4.0 International License. The images or other third party material in this article are included in the article's Creative Commons license, unless indicated otherwise in the credit line; if the material is not included under the Creative Commons license, users will need to obtain permission from the license holder to reproduce the material. To view a copy of this license, visit <http://creativecommons.org/licenses/by/4.0/>

© The Author(s) 2016

Supplementary Information accompanies the paper on the *npj Computational Materials* website (<http://www.nature.com/npjcompumats>)